Journal of Applied Fluid Mechanics, Vol. 10, No. 2, pp. 541-550, 2017.
Available online at www.jafmonline.net, ISSN 1735-3572, EISSN 1735-3645.
DOI: 10.18869/acadpub.jafm.73.239.26186

Numerical Simulation of Highly Charged Droplets Dynamics with Primary Break-up in Electrospray at Sub Rayleigh Limit

M. Rahmanpour[1†] and R. Ebrahimi[2]

[1] *Combustion and Propulsion Laboratory, Faculty of Aerospace Engineering, K.N. Toosi University of Technology, Tehran, Iran*
[2] *Department of Aerospace Engineering, K.N. Toosi University of Technology, Tehran, Iran*

†*Corresponding Author Email: mrahmanpour@dena.kntu.ac.ir*

(Received February 7, 2016; accepted November 17, 2016)

ABSTRACT

The size and the axial and radial velocity distributions of electrically controlled droplets generated from Taylor cone operating in the stable cone-jet regime are simulated by numerical modeling of electrosprays. A model is formulated as function of liquid flow rate, needle-to-counter electrode distance, applied voltage, and electrical conductivity and surface tension of the liquid in a DC electric field is presented with a 2D electrohydrodynamic model. The droplet size reduction can be explained by evaporation and/or Coulomb explosion. Results show that moving downstream, the average velocity of droplets decreases monotonically. This paper reports a numerical study of the effects of an externally applied electric field on the dynamics of drop formation from a vertical metal capillary. The fluid issuing out of the capillary is a viscous liquid, the surrounding ambient fluid is air, and the electric field is generated by establishing a potential difference between the capillary and a horizontal, electrode placed downstream of the capillary outlet. The Primary jet Break-up and droplet transport and evaporation of electrohydrodynamic sprays is investigated by modeling of droplet size and velocity distribution in spray cones and a series of drop migrations under the influence of an electric field were carried out and the results are in good agreement with other theoretical and experimental studies.

Keywords: Electro hydrodynamic; Electrospray; Primary break-up; Charged droplets; Rayleigh limit.

NOMENCLATURE

$\vec{B}$	magnetic flux
C_D	drag coefficient
D_{dif}	diffusion coefficient
d_i	droplet diameter
d_L	diameter of ligaments
d_0	jet diameter of liquid
d_{RR}	mean of the RR distribution
$\vec{E}$	electric field intensity
$\vec{E}_{ext}$	external electrical field vector
H	distance between nozzle and a plate
m	mass
N	total number of droplets
Oh	Ohnesorge Number
q_i	electrical charge
q_s	space charge density
$\vec{R}$	position vectors of droplet
Re	Reynolds Number
$\vec{v}$	droplet velocity vector
We	Weber Number
$Y_{d,S}$	mass fraction at the surface of droplet
$Y_{d,\infty}$	mass fraction in surrounding air
γ	surface tension of droplet liquid
ε_0	air electrical permittivity
ϵ	dielectric constant
λ_{opt}	wavelength of disturbances
μ_d	dynamic viscosity of droplet
ρ_d	droplet density
ρ_g	surrounding air density
ϕ_0	applied potential between nozzle and plate
ϕ	electric potential
ϱ	width of the RR distribution

1. INTRODUCTION

In electrospray, an electrical potential is applied between a nozzle and an electrode placed in the spray at a certain distance from discharge nozzle. As a result of the repulsion of like charges accumulated on the liquid surface, the jet surface becomes unstable and disrupts when the pressure due to the electrostatic forces exceeds the surface tension forces of the liquid. Droplets will be produced continuously if the electrical potential is increased above a critical value consistent with liquid flow rate (Ashkriz 2011).

A number of investigations have been made to explain the droplet formation mechanisms associated with electrostatic atomization (Gañán-Calvo *et al.* 2013, 2004, 1997). It has been hypothesized that the droplet size generated in electrostatic atomization is a function of applied electrical potential, electrode size and configuration, liquid flow rate, liquid nozzle diameter, and liquid properties such as surface tension, dielectric constant and electrical conductivity (Wilhelm 2004). As the applied electrical potential is increased, the droplets produce become smaller, and the liquid velocity and droplet production rate both increase, with concomitant shortening of the distance between adjacent droplets.

Generally, the liquid flow rates in electrostatic atomization are very low. This drawback has limited its practical applications. It should be noted that, to produce a reasonably monodisperse spray, the liquid flow rate should be maintained at an extremely low level, and thus the scaling up of such devices may pose some difficulties. It is also rather difficult to assess the liquid flow rate that can be achieved due to few quantitative studies and lack of comprehensive understanding of the underlying principles. Another drawback of the electrostatic atomization technique is that both the production and properties of droplets are significantly dependent on the electrical properties of the liquid, limiting the type of liquids that can be successfully atomized.

Droplet transport is investigated by few authors. The charged droplets follow the external electric field that is applied between the nozzle and the counter electrode. Gañán-Calvo *et al*. (1994) developed a Langragian numerical model for single droplet tracking between the droplet breakup location and the grounded counter plate. The results are compared to experimental droplet size and velocity values obtained with a Phase Doppler Anemometer (PDA). The axial droplet velocity is very high close to the capillary exit (~10m/s) and decrease towards the grounded plate following the decreasing electric field gradient. Due to the nature of the breakup the spray is very narrow close to the capillary exit but is spreading towards the plate due to the mutual repulsion of the charged droplets. The smaller droplets were pushed towards the spray edges due to their higher mobility. Hartman *et al.* (1999) used the model of Gañán-Calvo *et al.* (1994) but replaced the electric field approximation of Jones and Thong (1971) with their own electric field (Hartman *et al.* 1998) which is derived from a numerical calculation including the charge distribution on the cone. The comparison of the model to the experimental data shows similar underprediction of the axial droplet velocity as with Gañán-Calvo's model. The deficiency was explained by both authors by the entrained air due to momentum transfer from the droplets. Tang and Gomez (1994) examined the cone jet spray with a PDA as well. They found that the axial droplet velocity is mainly due to the external field whereas the radial spread of the spray comes from the mutual repulsion of the charged droplets. Their work also includes the only measurement of entrained air velocity in the cone jets. By measuring the velocity of uncharged alumina particles in the air stream they found that the air velocity takes values of about 30 – 40 % of the droplet velocity close to the capillary. The value is approaching zero close to the counter-plate.

Wilhelm (2004) in his PhD studied the transport, mass and heat transfer of charged droplets in the deposition of thin functional films. He used the same non-dimensional potential function that published by Gañán-Calvo *et al.* (1997) and did not solved exact governing equations on potential. Primary break-up model was not implemented and the break-up point, initial droplet size and it distribution are assumed monodisperse and the primary droplet size is calculated from the scaling laws of Gañán-Calvo *et al.* (1997). Also, in the second method that he called "initial conditions" since the initial droplet size and droplet velocity for the model calculation is taken from PDA measurements close to the nozzle.

One of the most important applications of the electrospray is Mass spectromy and carbon fiber-based ESI emitter. As an example, Sen *et al.* (2006a) simulated the carbon fiber-based ESI emitter using a computational fluid dynamics (CFD) software package FLOW3D. As it maintained before, one of the limitation of this spray is low flow rate. For this problem solution Sen *et al.* (2006b) simulate the multi-spray emitter.

This article is focusing on the development of a model describing the droplet transport and evaporation in a cone jet electrospray. Primary break-up model is used to determine the jet break up point and initial droplet size. The droplet mass transfer is controlled by evaporation and Raleigh breakup into small secondary droplets.

2. GOVERNING EQUATIONS

2.1 Droplet Transport

The motion of *i*th droplet emitted from an electrified meniscus towards a counter electrode is quantitatively described using Lagrangian droplet tracking of a dilute two-phase flow. The electrospray system is considered of droplets that do not interact with each other (dilute two-phase flow/one way interaction) and only columbic force and drag from the surrounding air act on them. Also, the air can be assumed to be still. Thus a force balance for transport of droplet ^{i} is written as:

$$\frac{\pi}{6} d_i^3 \rho_d \frac{d\vec{v_i}}{dt} = C_D \frac{\pi}{8} \rho_g d_i^2 \vec{v_i}^2 \vec{e_i} + q_i \vec{E}_{ext} + \frac{1}{4\pi\varepsilon_0} \sum_{ij,i\neq j}^{N} \frac{q_i q_j}{R_{ij}^3} \vec{R}_{ij} \quad (1)$$

where d_i is the droplet diameter, ρ_d is the liquid density (kg/m^3), ρ_g is the air density (kg/m^3), C_D is the drag coefficient, q_i is the electrical charge carried by ith droplet (C), $\vec{E}_{ext}$ is the external electrical field vector that created by the potential difference between the capillary tube and the plate (V/m), $\vec{R}_{ij} = \vec{R}_i - \vec{R}_j$ is displacement between the position vectors of droplets j ($\vec{R}j = (r_j, z_j)$) and i (m), ε_0 is the air permittivity (taken as 8.854×10^{-12} As/Vm), and N is the total number of droplets. The first term on the right hand side of this equation accounts for the drag force by the surrounding air, and it acts in the normal direction of droplet movement. The second term accounts for the force on the droplets by the external electric field between nozzle and grounded plate that acts in the direction of the electrical field. The third term accounts for the mutual electric forces between the charged droplets and the induced charge on the conductive substrate by the charged droplets (image force).

The terms on the right hand side (RHS) of Eq. (1) account for the drag force by the surrounding gas, the force on the droplets by the external electric field $\vec{E}_{ext}$ between nozzle and grounded plate, and the mutual electric forces between the charged droplets respectively. The drag coefficient C_D is written as (Clift *et al.* 1978):

$$C_D = \frac{24}{Re}(1 + 0.15\, Re^{0.678}), \quad Re < 800 \quad (2)$$

The path of i-th droplet can be followed through the velocity vector as:

$$\frac{d\vec{x}_i}{dt} = \vec{v}_i \quad (3)$$

It is assumed that the droplets are moved in still air following Gañán-Calvo *et al.* (1994) who calculated the air to droplet velocity ratio to be far smaller than unity. The external electric field calculation will be described in details.

2.2 Droplet Evaporation

Droplets expose to evaporation on their trajectory from the nozzle to the counter plate and their size reduces during transportation. We obtain the droplet radius (or diameter) history by writing a mass balance that states that the rate at which the mass of the droplet decreases is equal to the rate at which the liquid is vaporized;

$$\frac{dm_d}{dt} = -\dot{m} \quad (4)$$

where the droplet mass, m_d, is given by:

$$m_d = \rho_d \pi {d_d}^3/6 \quad (5)$$

According to Stephan problem for single droplet evaporation Turns (2011, 2006) propose evaporation rate as:

$$\frac{dd_d}{dt} = -4 \frac{\rho_a}{\rho_d} \frac{D_{dif}}{d_d} \ln(1 + B_Y) \quad (6)$$

where D_{dif} is diffusion coefficient (m^2/s) of droplet to air and B_Y is dimensionless transfer number that can be define as:

$$B_Y = \frac{Y_{d,S} - Y_{d,\infty}}{1 - Y_{d,S}} \quad (7)$$

where $Y_{d,S}$ and $Y_{d,\infty}$ are mass fraction at the surface of droplet and mass fraction of in surrounding air respectively.

All properties of the air-solvent gas mixture in the film boundary layer around the droplet can be assumed constant if they are calculated at reference temperature and at reference composition. These values are evaluated according to the 1/3 rule of Sparrow and Greg (1958).

2.3 Electric Field Equations

The study of electric field effects on dielectric media requires knowledge of the distribution of electric field as well as electric potential. In principle the electric potential distribution within the system under applied electric fields may be determined using Poisson's equation provided that the dielectric constant is held constant:

$$\nabla^2 \phi = -\frac{q_s}{\varepsilon} \quad (8)$$

where ϕ, q_s, ε denote electric potential, space charge density, electrical permittivity respectively.

There is no bulk free charge density in dielectric fields unless a given element of dielectric media can be traced via its stream line to a source of charge. If this is the case then the Poisson's equation is reduced to Laplace's equation:

$$\nabla^2 \phi = 0 \quad (9)$$

We consider the electro-quasi-static case, where the magnetic flux $\vec{B}$ does not change with time. Due to Faraday's law of induction $-\frac{\partial \vec{B}}{\partial t} = \text{curl}\ \vec{E}$ the curl of the electric field vanishes

$$\text{curl}\ \vec{E} = \nabla \times \vec{E} = 0 \quad (10)$$

where $\vec{E}$ (V/m) is the electric field intensity. According to Eq. (10), the irrotational nature of the electric field intensity indicates that there is a scalar function ϕ (electric potential) related with the electric field intensity (See Castellanos 1998 for details)

$$\vec{E} = -\nabla \phi \quad (11)$$

In this study, Eq. (9) has been solved for geometry of nozzle and a plate with distance H and a high potential ϕ_0 applied between nozzle and extractor and then electric field intensity could be calculated by Eq. (11). In Fig. 1 the electric potential distribution in the whole domain is illustrated. As observed, the equipotential lines get closer at the vicinity of the jet tip demonstrating that the potential gradient is high in this region. Also Fig. 2 shows the Electric Field Vector ($\vec{E}$) in the zoomed view near to the nozzle tip. It is clearly shows that the electric forces ($q\vec{E}$) force the fluid to change to a conical shape and focuses the jet and results a thin jet and

fine droplets as it effects. Also, the velocity field vector inside the liquid for the case shown in Fig. 3. It can be seen, as a result of electric forces, at the capillary exit, fluid changes to a conical shape and a thin jet found at its apex.

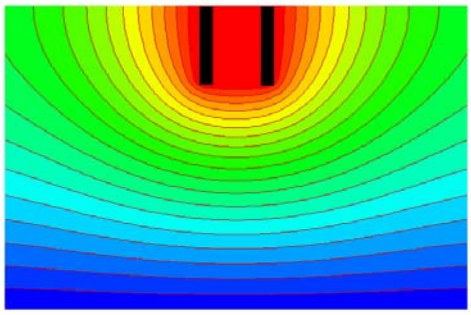

Fig. 1. Electric potential distribution contour in the domain.

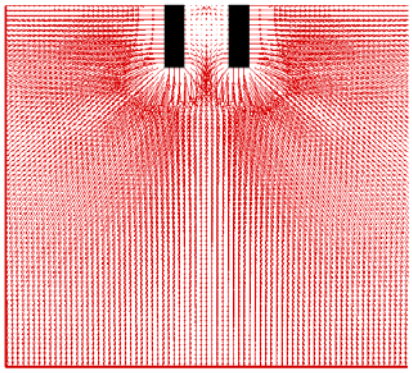

Fig. 2. Field Vector ($\vec{E}$) in the zoomed view near to the nozzle tip.

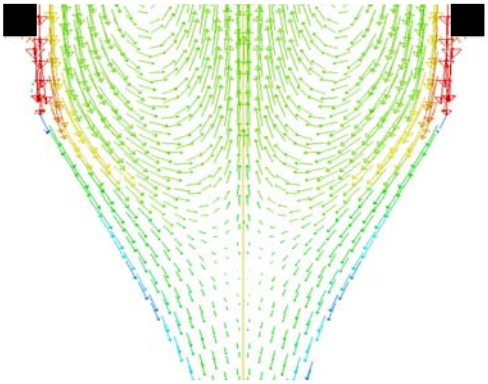

Fig. 3. Velocity Vectors in the zoomed view near to the nozzle tip.

Also, the velocity field, inside the liquid cone is shown. It can be seen that the velocity vectors extend outside the jet. In the velocity field, a vortex can be seen. The liquid moving down in the main flow direction is divided by the vortex. In each side, the majority of the liquid is drawn back into the centre vortex and is re-circulated and mixed with the main flow. The remaining liquid is drawn into the jet. Hayati *et al.*(1987) studied the flow pattern inside the liquid cone using illuminated particles and photographing the dynamics of these particles. They observed axi-symmetric circulating patterns inside the cone. Particles were observed moving down along the surface towards the cone apex and then turning and moving up along the symmetry line. These results are consistent with the back flow seen in the CFD results (Rahmanpour *et al.* 2015). In the jet, the liquid undergoes a strong acceleration to reach an equilibrium velocity after a short distance downstream. Details of numerical simulation of Electric Field Equations and CFD Simulation of Taylor cone jet, can be found in Najjaran *et al.* 2013 and Rahmanpour *et al.* 2015 .

2.4 Primary Break-Up Model

It is generally accepted that an aerodynamic instability causes the jet to break up. The mathematical analysis below assumes that Kelvin-Helmholtz waves grow on the sheet and eventually break the liquid into ligaments. It is then assumed that the ligaments break up into droplets due to varicose instability (Madsen 2006).

The model used in this study is called the Linearized Instability Sheet Atomization (LISA) model of Schmidt *et al.* (2000). The model includes the effects of the surrounding gas, liquid viscosity, and surface tension on the breakup of the liquid sheet. Details of the theoretical development of the model are given in Madsen (2006) and are only briefly presented here.

The model assumes that a two-dimensional, viscous, incompressible liquid sheet of thickness 2h moves with relative velocity U through an inviscid, incompressible gas medium. The liquid and gas have densities of ρ_d and ρ_g, respectively, the viscosity of the liquid is μ_d and surface tension is γ.

Squire (1953) has shown that two solutions, or modes, exist that satisfy the liquid governing equations subject to the boundary conditions at the upper and lower interfaces. For the first solution, called the sinuous mode, the waves at the upper and lower interfaces are in exactly phase. On the other hand, for the varicose mode, the waves are π radians out of phase (see Fig. 4). It has been shown by numerous authors, e.g. Senecal *et al.*, (1999), that the sinuous mode dominates the growth of varicose waves for low velocities and low gas-to-liquid density ratios. In addition, it can be shown that the sinuous and varicose modes become indistinguishable for high-velocity flows. As a result, in the present article focuses on the growth of sinuous waves on the liquid sheet.

2.4.2 Ligament Formation

The diameter of ligaments formed at the point of breakup can be obtained from a mass balance.

The ligament diameter is assumed to be linearly proportional to the wavelength, Λ_S, which breaks up the sheet (Fluent, 2005):

$$d_L = C_L \Lambda_S = \frac{2\pi C_L}{K_S} \tag{15}$$

where C_L is a ligament constant. And K_S is the most unstable wave number and then given by

$$K_S = \frac{\rho_g U^2}{2\gamma} \tag{16}$$

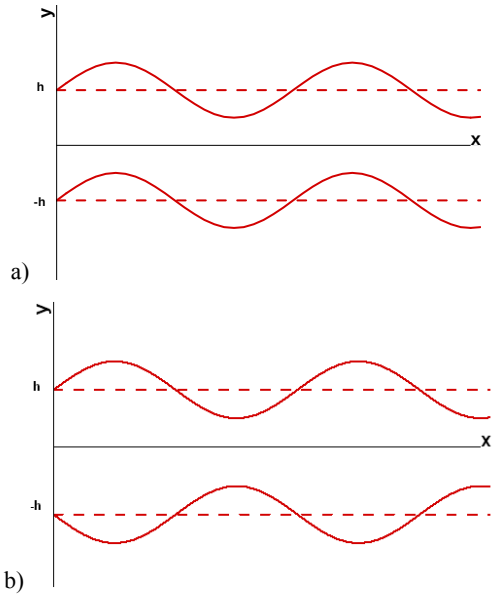

Fig. 4. Schematic of (a) antisymmetric or sinuous waves and (b) symmetric or varicose waves.

2.4.3 Drop Formation

In either the short wave or the long wave case, the breakup from ligaments to droplets is assumed to behave according to Weber's analysis for capillary instability (Dombrowski and Johns 1963). The wave number, K_L, corresponding to the maximum growth rate for the breakup of a cylindrical, viscous column is determined from

$$K_L d_L = \left[\frac{1}{2} + \frac{3\mu_d}{2(\rho_d \gamma d_L)}\right]^{-1/2} \tag{17}$$

If it is assumed, as in Dombrowski and Johns (1963), that breakup occurs when the amplitude of the unstable waves is equal to the radius of the ligament; one drop will be formed per wavelength. Thus by mass balance the relation between drop size and wave number is given by

$$d^3 = \frac{3\pi {d_L}^2}{K_L} \tag{18}$$

for the drop size d_D, which on combination with Eq. (17) gives

$$d_D = 1.88 d_L (1 + 3Oh)^{1/6} \tag{19}$$

where Oh is the Ohnesorge number, which is a combination of Reynolds number and Weber number:

$$Oh = \frac{\sqrt{We_d}}{Re_d} = \frac{\mu_d}{\sqrt{\rho_d \gamma d_L}} \tag{20}$$

In the above models, it is assumed that the liquid sheet has been atomized into discrete droplets at the exit of the nozzle. Hence, a size distribution has to be used with the mean droplet size given by the sheet thickness. A Rosin-Rammler distribution was used by Schmehl *et al.* (2000).

In studies of sprays, Schmidt *et al.* (2000) and Senecal *et al.* (1999) used the LISA method to give the initial droplet size, d_D, at the breakup location. Nagaoka and Kawamura (2001) and Rotondi and Bella (2006) used another sheet atomization model based on the linear sheet instability argument. They estimated the initial droplet sizes and the breakup length from the stability analysis performed by Dombrowski and Johns (1963).

In our models, it is assumed that after the liquid sheet breaks up, the sizes of the droplets are distributed according to a Rosin-Rammler distribution with a spread parameter of $\varrho = 3.5$.

2.4.4 Rosin Rammler Distribution

Most commonly used size distribution functions represent simplifications of modifications of the Nukiyama-Tanasawa function (Lefebvre, 1989). One example is the normalized form of the Rosin-Rammler distribution:

$$f_0(d) = \frac{\varrho}{d_{RR}\Gamma(1-3/\varrho)}\left(\frac{d}{d_{RR}}\right)^{\varrho-4} \exp\left[-\left(\left(\frac{d}{d_{RR}}\right)^{\varrho}\right)\right] \tag{21}$$

where d_{RR} represents the mean of the distribution, and ϱ indicates the value of the width of the distribution. Small values of ϱ are associated with broad sprays, and large values of ϱ are associated with narrow sprays. Usually $1.5 < \varrho < 4$ (Lefebvre, 1989). The Rosin-Rammler distribution gives a good fit to droplet volume distributions for sprays; however, it often gives a rather poor fit to the droplet number distribution (Nasr *et al.*, 2002). In this study, mean droplet size found from Eq. (19) and used 4% for standard deviation according to experimental results.

Clearly, the mean droplet size decreases with increasing electric field intensity, dielectric constant, and/or liquid surface tension, but increases with increasing liquid flow rate, liquid density, liquid viscosity, and/or liquid supply tube diameter. The effects of liquid surface tension and liquid supply tube diameter appear less significant in electrostatic atomization (Huimin Liu, 2000).

2.4.5 Rayleigh Limit

In 1882, Lord Rayleigh theoretically estimated the maximum amount of charge a liquid droplet could carry, this is now known as the "Rayleigh limit". The solvent evaporates from a charged droplet until it becomes unstable upon reaching its Rayleigh limit. At this point, the droplet deforms as the electrostatic repulsion of like charges, in an ever-decreasing droplet size, becomes more powerful than the surface tension holding the droplet together. At this point the droplet undergoes Coulomb fission, whereby the original droplet explodes creating many smaller, more stable droplets. During the fission, the droplet loses a small percentage of its mass (1.0–2.3%) along with a relatively large percentage of its charge (10–18%)

In accordance with Rayleigh instability, fission of the charge droplets would occur when:

$$q_i \geq 8\pi\sqrt{\varepsilon_0 \gamma R_i^3} \tag{22}$$

where γ is the surface tension. In this research the droplet size, applied voltage and liquid properties are chosen such that the droplets to be stable and Columbic Fission does not occur (sub Rayleigh limits). The instances where charged droplets have been reported to break-up at charge levels other than predicted by Rayleigh theory have been shown to be the result of droplet contamination or an incorrectly determined charge level. As such, Rayleigh theory is currently held as valid for charged droplets that are purely liquid in phase and are stably levitated (Cook Hunter, 2011).

3. NUMERICAL PROCEDURE

To couple the electrohydrodynamic body force to the momentum equation, first a second-order partial differential equation (Eq. (9)) is solved to obtain the potential field $\phi(r,z)$. Mean droplet size, frequency and break-up points can be found from using of the equations of section 2.4. Then Rosin-Rammler distribution function is used and the droplet beak-up time can be calculated from the continuity. Now, equation is solved for droplets and the droplet size change in every time steps by using evaporation equations. At any time Rayleigh Limit is checked.

4. RESULTS AND DISCUSSION

First, the Taylor cone and resulting jet was simulated using the VOF model presented in Rahmanpour *et al.* (2015). The resulting jet diameter (54μm), average droplet diameter (using Eq. (19), 28.2μm and 4% standard deviation), average droplet speed (using continuity and droplet size, 20.9 m/s), charge density (67.2 C/m), primary break-up point (one height of the Taylor cone plus three wave lengths, Eq. (5)) and frequency (110 Hz) of the primary droplet were simulated and utilized in the simulation of droplet transportation process. At a distance of 2.6 cm downstream from the droplet inlet boundary, a comparison of the average droplet diameter and average axial velocity versus radial distance from the spray center predicted by the model and measured from experiments is depicted in Fig. 5-6. Because the surface to volume ratio in smaller droplets is higher, smaller droplet diameter leads to faster evaporation. The model results have good agreement with the experimental data in terms of droplet size within 7% and droplet velocity value within 10%. However, droplet velocities predicted by the model are higher than the experimental values and these differences are more in high droplet velocities. This may be due to the results of negligible air-phase velocity assumption.

Due to decrease in the size of the droplet as it moves through the spray core, as a result of evaporation, the surface charges are brought closer and the repulsive force between the charges increase. When the Coulombic force exceeds the surface tension force the droplet breaks into smaller droplets (Columbic Fission). In accordance with Rayleigh instability, fission of the charge droplets would occur when:

$$R_i \leq R_R \tag{23}$$

Where

$$R_R = \frac{{q_i}^{2/3}}{\sqrt[3]{16\pi^2\varepsilon_0\gamma}} \tag{24}$$

In Fig. 5, dash line shows this Rayleigh Limit droplet size (R_R). If the droplet size reaches to this limit, columbic fission takes place and breaks into smaller droplets. It can be seen that all droplets are greater than this limit in every positions in this case study.

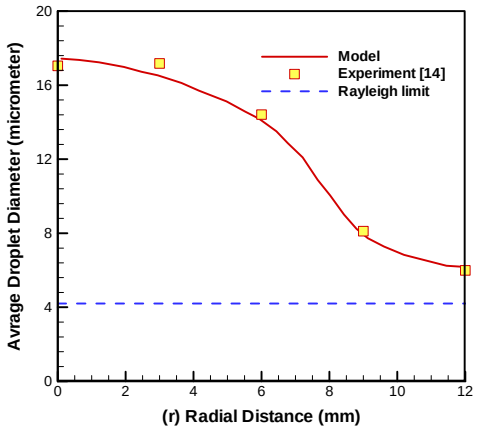

Fig. 5. Comparison of average droplet diameter obtained from the Model and measured from experiments Shrimpton (2008).

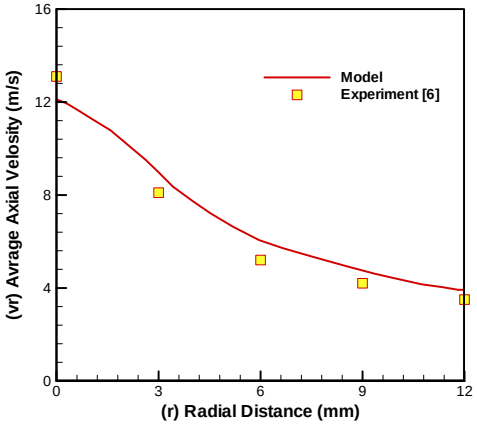

Fig. 6. Average droplet diameter vs. axial velocity obtained from the simulation and measured from experiments Hartman (1998).

A small time step size of 1.6×10^{-7} sec was used that accurately capture the droplet breakup process. The steady state was obtained by observing no change in the total numbers of the droplets in physical domain.

In all modeling procedure Rayleigh limit for this droplet can be calculated from Rayleigh (1879):

$$q_R = 8\pi(\gamma\varepsilon_0 d^3/8)^{1/2} \quad (22)$$

Furthermore, accounting for the Rayleigh limit of charging during evaporation may change the final droplet size and even contribute to production of ultrafine satellite droplets. In droplet migration, charge density assumed to be constant and in each step droplet diameter checked by Rayleigh limit.

In Fig. 7, the snapshot of droplets location distribution of the electrospray plume is presented, where each point represents a single droplet. The results show that there are 3520 droplets present in the spray at steady state. It is clearly seems that the mutual repulsion of the charged droplets lead to increase the spread of the spray with increasing distance from the jet breakup point. Also, the spray half angle that calculated by the model simulation is 34.1 approximately and that measured from experiments is 35.9. Also, due to surface evaporation during trajectory, the droplet diameter will be decreased and reach to Rayleigh limit. As predicted, the droplets at the edge of spray plume are smaller and therefore the possibility of reaching to Rayleigh limit is more. In Fig. 6, green circles (not filled green points) show the droplets that reached to Rayleigh limit and should break-up to sibling droplets. This process known as coulomb fission and did not simulated here and its details explained in Clift et al. (1978). It seems that, because fission process did not model here, the spray plume angle calculates smaller than the experiment.

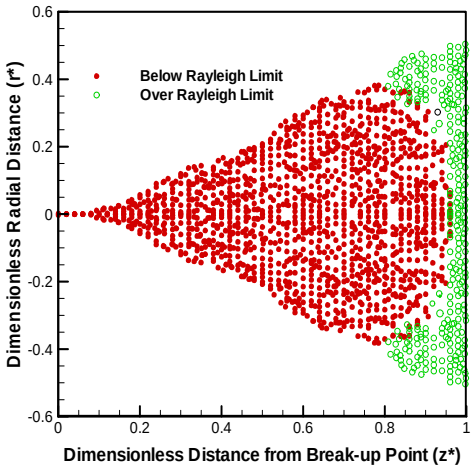

Fig. 7. A steady-state snapshot of droplets location distribution of the electrospray plume with $z^* = \frac{z}{H}$ and $r^* = \frac{r}{H}$.

Figure 8 illustrates the variation of average axial velocity in the radial direction at three different axial locations is presented. It is clearly observed that because of the higher electrical force at the spray center, the droplets migrate faster at the spray center as compared to the edges. Also, the velocity profiles flatten as the spray approaches the substrate plate. This is because the electric field in the spray close to the counter electrode has the less influence on the droplets. Similar results have been reported by Gañán–Calvo *et al.* (1994, 1997), Wilhelm (2004) and Kumar Sen *et al.* (2011) both from model and experiments.

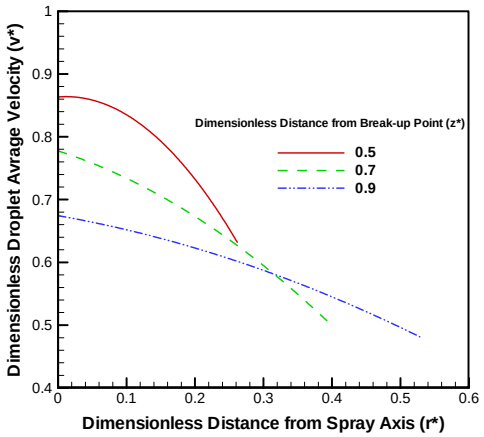

Fig. 8. Variation of the average droplet axial velocity along z-direction.

Figure 9 shows the radial droplet size distribution at various distances from breakup point. The results show that the average droplet diameter remains rather constant in the radial direction but due to evaporation and second breakup the average droplet diameter decrease.

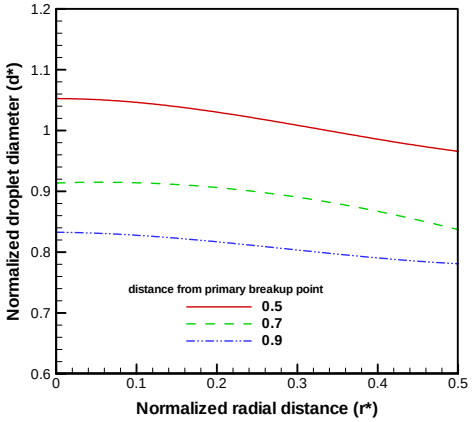

Fig. 9. Variation of the average droplet diameter along z-direction.

In Fig. 10, the variation of Spray plume angle with applied voltage change has been showed. As it can be seen, spray plume angle increase logarithmically with increase of the applied voltage because applied voltage increases lead to more surface charge density and in the effect or mutual charge force the plume angle will be increased.

Figure 11 shows droplet size distributions at different locations along the spray axis. In Fig. 10(a) clearly we can observe that the size distribution is initially very monodisperse, with a ratio of standard deviation (SD) over average diameter (D_{avr}), SD/D_{avr}, equal to 0.00118. droplet size distributions are in fairly good agreement with a Gaussian distribution. So we can summarize our data using the

mean value and the standard deviation and easily (Artana et al. 1998).

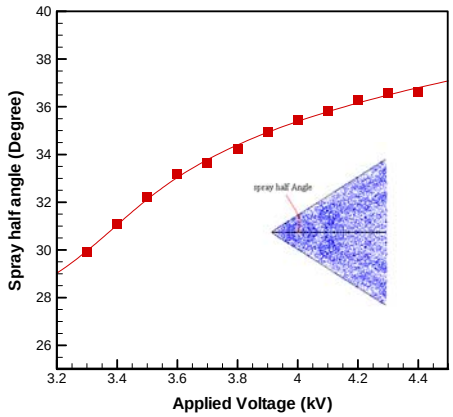

Fig. 10. Spray plume angle variation with Applied Voltage (Triethylene Glycol (TEG)+NAI, Solution Conductivity (K)=0.01 S/m, Emitter Out Diameter(OD)=0.56 mm, Capillary-Grid Spacing=3 mm, Nominal Flow rate=120 nL/s).

Compare the electrified and non-electrified cases. Further downstream, as droplets begin to evaporate and migrate to extractor, the size distribution broadens (Fig. 10(a) ($SD/D_{avr} = 0.00226$) with a longer "tail" developing in the small size range. In addition, with attention to the small standard deviation values given in this figures show that the distribution of the droplets in the Electrospray is uniform and near to the monodisperse (Fig. 10(a-d)). Also, comparison of average diameter in different distance from break-up point indicates that due to surface evaporation droplet diameter reduce and fine droplets will be produced.

Figures 1 and 2 show electric potential distribution in the whole domain at time t=0. In the other times with forming of jet and, due to surface charge density, electric potential distribution will be change. But the change effects are not significant as shown in Fig. 12.

5. CONCLUSION

Detailed simulations of the droplets dynamics of an electrospray plume have been performed for modeling of transport and evaporation of electrosprayed droplets in the sub Rayleigh limit. The model was in reasonably good agreement with a literature model of electrospray transport and droplet evaporation. Results show that moving downstream, the average velocity of droplets decreases monotonically. Also, evaporation affects the electrospray droplet transport and it can strongly reduce droplet size. It was shown also that electrospraying may lead to wide spray plume angle resulting from the mutual repulsion of droplets. Evaporation does not dramatically alter electrospray droplet transport but it can drastically reduce droplet size and increase salt concentration affecting.

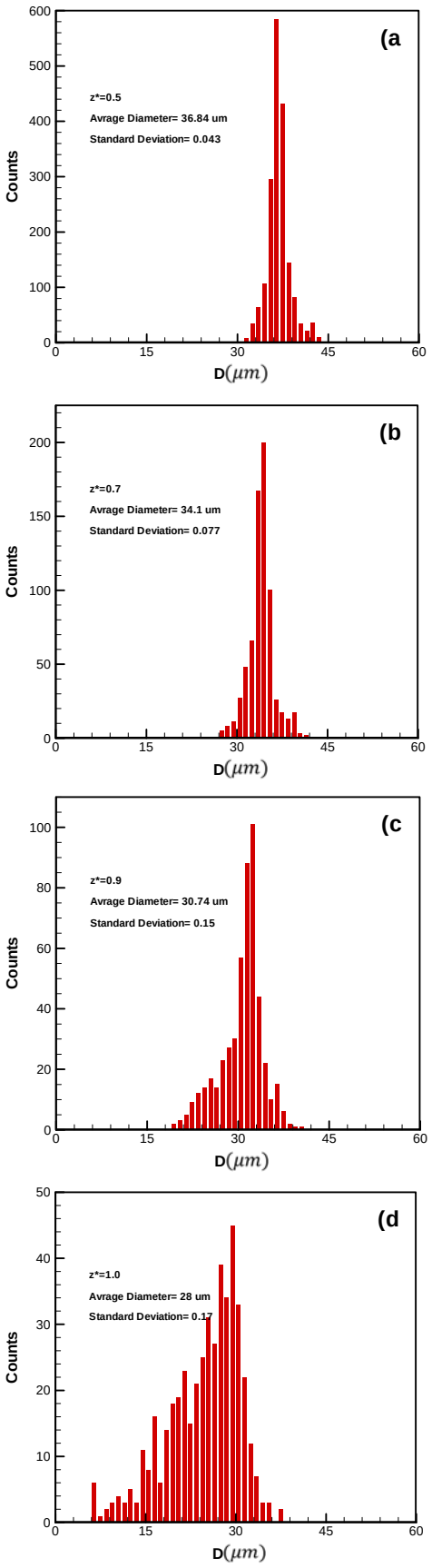

Fig. 11. Size distributions of an evaporating spray at various locations along the spray axis: (a) $z^* = 0.5$, (b) $z^* = 0.7$, (c) $z^* = 0.9$, and (d) $z^* = 1.0$.

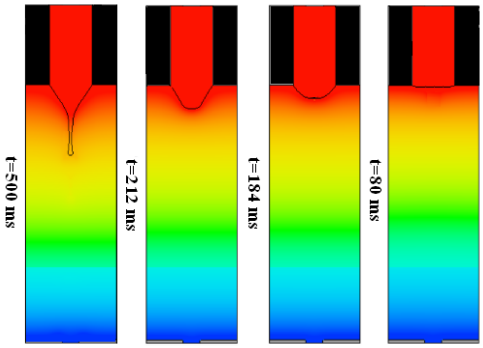

Fig. 12. Taylor cone and jet profiles with electric potential contours in the computational domain in some time steps.

It was shown also that electrospraying may lead to non-uniform deposits resulting from the mutual repulsion of droplets. Furthermore, accounting for the Rayleigh limit of charging during evaporation may change the final droplet size and even contribute to production of ultrafine satellite droplets and fine nano-particle deposits that may degrade the film quality. Furthermore, accounting for the Rayleigh limit of charging during evaporation may change the final droplet size and even contribute to production of ultrafine satellite droplets.

The initial droplet size, break-up frequency, and break-up location point are important parameters in spray plume, and could affect the spray properties. So, achieving to the appropriate Primary Break-up method is necessary. The method that used here has good capability to solve such cases and the results are in good agreements with experiments.

Application of the model facilitates the simulation of different electrospraying modes and finding the conditions under which cone-jet mode occurs, all of these can be subjects for future works.

REFERENCES

Artana, G., H. Romat and G. Touchard (1998). Study of a high-velocity liquid jet stressed by an electric field. *Physics of Fluids* 10(11), 2922-2931.

Ashkriz, N. (2011), *Handbook of Atomization and Sprays: Theory and Applications*. Springer.

Castellanos, A. (1998). *Electrohydrodynamics*. Springer-Verlag Wien.

Clift, R., J. R. Grace and M. E. Weber (1978). *Bubbles, Drops, and Particles*. Academic Press, New York, USA.

Dombrowski, N. and W. R. Johns (1963). The aerodynamic instability and disintegration of viscous liquid sheets. *Chemical Engineering Science* 18(3), 203-214.

Fluent (2005), *Fluent 6.2 User's Guide*, Fluent Inc., Lebanon, NH.

Gañán –Calvo, A. M. (1994). The electrostatic spray emitted from an electrified conical meniscus. *Journal of Aerosol Sci.* 25(6), 1121-1142.

Gañán –Calvo, A. M., J. Davila and A. Barrero (1997). Current and droplet size in the electrospraying of liquids. *Journal of Aerosol Sci.* 28(2), 249-275.

Gañán-Calvo, A. M. and J. M. López (2004). A Note on Charged Capillary Jet Breakup of Conducting Liquids: Experimental Validation of a Viscous One Dimensional Model. *J. of Fluid Mechanics* 501, 303-326.

Gañán-Calvo, A. M., N. Rebollo-Muñoz and J. M. Montanero (2013). The Minimum or natural rate of flow and droplet size ejected by taylor cone-jets: physical symmetries and scaling laws. *New Journal of Physics* 15(3), 33-35.

Gomez, A. and K. Tang (1994). Charge and fission of droplets in electrostatic spray. *Phys. Fluids* 6(1), 404-414.

Hartman, R. (1998). *Electrohydrodynamic atomization in the cone-jet mode. From physical modeling to powder production*. Ph.D. Thesis, the TU Delft University, Delft, Netherland.

Hartman, R. P. A., J. P. Borra, D. J. Brunner, J. C. M. Marijnissen and B. Scarlett (1999). The evolution of electrohydrodynamic sprays produced in the cone-jet mode, a physical model. *J. of Electrostatics* 47(3), 143-170.

Hayati, I., I. A. Bailey and T. F. Tadros (1987). Investigation into the mechanism of electrohydrodynamic spraying of liquids. *Journal of Colloid and Interface Science* 117(1), 222–230.

Hunter III, H. C. (2011). *Studies Related to Coulombic Fissions of Charged Droplets and Hygroscopic Behavior of Mixed Particles*. Ph. D. thesis, The Graduate School, University of Kentucky, USA.

Jones, A. R. and K. C. Thong (1971). The production of charged monodisperse fuel droplets by electrical dispersion. *Journal of Physics D: Applied Physics* 4(8), 1159–1166.

Lefebvre, A. H. (1989). *Atomization and Sprays*. Hemisphere, New York, USA.

Liu, H. (2000). *Science and Engineering of Droplets*. William Andrew Publishing, LLC, Norwich, New York, USA.

Madsen, J. (2006). *Computational and Experimental Study of Sprays from the Breakup of Water Sheets*. Ph. D. thesis, Faculty of Engineering and Science, Aalborg University, Denmark.

Mori, Y., K. Hijikata and T. Nagasaki (1981). Electrostatic atomization for small droplets of uniform diameter. *Trans. Jpn. Soc. Mech. Eng. Ser. B* 47, 1881–1890.

Nagaoka, M. and K. Kawamura (2001). A deforming droplet model for fuel spray in direct-injection gasoline engines. *SAE Technical Paper 2001*, 01, 1225.

Najjaran, A. K., R. Ebrahimi, M. Rahmanpoor and A. Najjaran (2013). Numerical simulation of electrohydrodynamic (EHD) atomization in the cone-jet mode. *Applied Mechanics and Materials* 325-326, 180-185.

Nasr, G. G., A. J. Yule and L. Bendig (2002). *Industrial Sprays and Atomization*. Springer, London, UK.

Rahmanpour, M. and R. Ebrahimi (2015). Numerical simulation of electrohydrodynamic spray with stable Taylor cone–jet. *Heat and Mass Transfer* 51(10), 1-9.

Rayleigh, L. (1879). On the conditions of instability of electrified drops. *Proc. Roy. Soc.*, 29, 71-83.

Rotondi, R. and G. Bella (2006). Gasoline direct injection spray simulation. *International Journal of Thermal Sciences* 45(2), 168-179.

Schmehl, R., G. Maier and S. Wittig (2000). CFD analysis of fuel atomization, secondary droplet breakup and spray dispersion in the premix duct of a LPP combustor. *Proc. ICLASS 2000*, 918-925.

Schmidt, D. P. and C. J. Rutland (2000). A new droplet collision algorithm. *Journal of Computational Physics* 164(1), 62-80.

Sen, A. K., J. Darabi and D. R. Knapp (2007). Simulation and parametric study of a novel multi-spray emitter for ESI–MS applications. *Microfluid Nanofluid* 2, 283-298

Sen, A. K., J. Darabi and D. R. Knapp (2011). Aerosol formation in electrospray ionization using a micro fluidic emitter. *IEEE Sensors Journal* 11(10), 2335-2341.

Sen, A. K., J. Darabi, D. R. Knapp and J. Liu (2006). Modeling and characterization of a carbon fiber emitter for electrospray ionization. *Journal of Micromech. Microeng.* 16(3), 620–630.

Senecal, P. K., D. P. Schmidt, I. Nouar, C. J. Rutland, R. D. Reitz and M. L. Corradini (1999). Modeling high-speed viscous liquid sheet atomization. *Int. J. Multiphase Flow* 25(3), 1073-1097.

Shrimpton, J. S. (2008). Modeling dielectric charged drop break up using an energy conservation method. *IEEE Transactions on Dielectrics and Electrical Insulation* 15(5), 108-120.

Sparrow, E. M. and J. L. Gregg (1958). The variable fluid-property problem in free convection. *Transactions of the ASME* 80, 879–886.

Squire, H. B. (1953). Investigation of the instability of a moving liquid film. *British Journal of Applied Physics* 4, 167-169.

Turns, S. R. (2006). *Thermal-Fluid Sciences: An Integrated Approach*. Cambridge University Press, England.

Turns, S. R. (2011). *An Introduction to Combustion: Concepts and Applications*. 3rd ed., McGraw-Hill Education, New York, USA.

Wilhelm O. (2004). *Electrohydrodynamic Spraying –Transport, Mass And Heat Transfer Of Charged Droplets And Their Application To The Deposition Of Thin Functional Films*. Ph. D. thesis, the University of Tübingen, Zurich, Switzerland.